

# INCREASING SPATIAL RESOLUTION OF SEA ICE MOTION ESTIMATION

Zisis I. Petrou<sup>1</sup>, Yang Xian<sup>2</sup>, and YingLi Tian<sup>1,2</sup>

<sup>1</sup>Department of Electrical Engineering, The City College of New York,  
The City University of New York, New York, NY 10031, USA

<sup>2</sup>Department of Computer Science, The Graduate Center,

The City University of New York, New York, NY 10016, USA

E-mails: {zpetrou,ytian}@ccny.cuny.edu, yxian@gradcenter.cuny.edu

## ABSTRACT

Estimation of sea ice motion at a fine scale is essential for climate modeling and naval operations in polar regions. This study proposes an approach for increasing the spatial resolution of the motion estimated from passive microwave satellite images. A hierarchical pattern matching approach, based on normalized cross-correlation and phase correlation, is applied to calculate sea ice drifts between Advanced Microwave Scanning Radiometer 2 (AMSR2) pairs of images captured at different time. Contrary to the widely used approach of embedding oversampling within the pattern matching framework that increases the resolution of the minimum detectable drift, in this study a nearest-neighbor interpolation upscaling is applied directly to the images. This additionally increases the density of the estimated motion vectors. Experiments demonstrate that the proposed method can lead to motion vector field with increased resolution by up to eight times, while outperforming the original images. Image upscaling by four times also outperforms corresponding previous examples with embedded oversampling.

**Index Terms**— Advanced Microwave Scanning Radiometer 2 (AMSR2), hierarchical maximum cross-correlation (MCC), image upscaling, motion tracking, phase correlation (PC), sea ice drift estimation

## 1. INTRODUCTION

Sea ice motion is an important component in modeling ocean-atmosphere interactions and safeguarding naval activities in polar regions, including ship navigation, fisheries, and oil and gas exploration [1]. Motion estimation from satellite imagery at a fine scale is essential in these applications [2].

Images from passive microwave satellite data have been widely used for sea ice motion estimation in research studies and operational products [3–6]. Their main advantages over optical data include insensitivity to cloud contamination and lack of sun illumination, and over Synthetic Aperture Radar

(SAR) data large swath widths that allow daily coverage of the polar regions. However, the spatial resolution of passive microwave sensors is rather coarse, i.e., around 5–25 km.

Sea ice motion estimation, including with passive microwave data, has mainly been performed with pattern matching methods, mostly based on maximum cross-correlation (MCC), and more recently, phase correlation (PC) [7–9]. For each pair of images, from the same area but captured at different time, the first image is split into overlapping or non-overlapping *templates* (i.e., image subregions, also called *patches*) and then each template is searched in the second image to find the one that best matches the pattern of the former one. The relative distance and direction from the first to the second matching template forms a motion vector that represents the corresponding sea ice drift. Such motion vectors are calculated for all templates of the first image. As readily inferred, the minimum motion is one pixel, i.e., it is quantized to the image resolution. Some studies have attempted to reduce this quantization error. In [3, 6], an implicit linear interpolation step was applied to perform oversampling that reduced the minimum detected drift by four times compared with the original image resolution. Curve fitting in the correlation value domain was applied in [10], whereas bilinear interpolation followed by continuous optimization was proposed in [4]. Although the authors decreased the minimum detected motion attempting to reduce the quantization error, the density of the motion vector field, i.e., the number of calculated motion vectors per unit area, remained the same.

In this study, we propose to directly upscale the spatial resolution of the image data. This is expected to increase the spatial resolution of the detected motion as well as the density of the motion vector field, since more image pixels ensure more templates to cover the same sea area, for a fixed template size in pixels. In addition, since the upscaling step is performed independently of the core motion estimation algorithm, the proposed approach allows flexibility on the selection or design of the motion estimation algorithm. In this study, the use of a simple nearest-neighbor (NN) interpolation is investigated, followed by motion estimation based on

a hierarchical MCC and PC approach.

## 2. DATA

Advanced Microwave Scanning Radiometer 2 (AMSR2) data acquired from the JAXA Earth Observation Research Center<sup>1</sup> are employed in this study. In particular, level 1R daily averaging images of horizontal polarization 36.5 GHz brightness temperature data are used. The data are gridded on a polar stereographic grid, tangent to the Earth's surface at 70 degrees northern latitude, with 12.5 km spatial resolution [11]. Seven images from January 1–7, 2013, are employed, covering the entire Arctic region, with the latitude-longitude coordinates of the image corners being: top-left (30.98°N, 168.35°E); bottom-left (33.92°N, 80.74°W); top-right (31.37°N, 102.34°E); bottom-right (34.35°N, 9.97°W).

In order to conduct the motion estimation on the sea ice regions of the image area, a sea ice mask is generated from the Multisensor Analyzed Sea Ice Extent - Northern Hemisphere (MASIE-NH) product [12]. The product is based on visible imagery, passive microwave data, and weekly analysis products of the National Ice Center (NIC). In particular, the MASIE-NH product of 4 km resolution from January 1, 2013, is employed for consistency. The sea ice mask is reprojected to the 12.5 km polar stereographic grid of the AMSR2 images and clipped to the extent of the images.

## 3. METHODOLOGY

### 3.1. Image upscaling

A simple NN interpolation is applied to create upscaled versions of the AMSR2 images as well as the MASIE-NH sea ice mask. NN is selected in order to avoid generating intermediate interpolated brightness temperature values that may cause unwanted smoothing of the image edges that can burden the forthcoming pattern matching process. The AMSR2 images—and the sea ice mask—are upscaled by two, four, and eight times, resulting in images with pixel spatial resolution of 6.25 km, 3.125 km, and 1.5625 km, respectively.

### 3.2. Motion estimation

The sea ice motion is estimated with a hierarchical MCC-based approach inspired by [7, 8] and presented in detail in [13]. Following the pattern matching method paradigm, for each template in the first image of an image pair, the method searches for the best matching template in the second one. PC value (Eq. (2) in [13]) is initially calculated in the frequency domain, to quickly identify candidate motion distances and directions around the neighborhood of the first template on the second image. The Normalized Cross-Correlation (NCC) criterion (Eq. (1) in [13]) is then applied for the candidate

drifts with PC value >25% of the maximum PC value. The final drift is selected as the one with the maximum NCC value.

The method involves a multiresolution and multicascade approach to reduce the searching space and speed up the pattern matching process. For a set of input images—which can be either the original images or the upscaled by NN ones—the multiresolution approach indicates the creation of an image pyramid, downscaling at each pyramid level the images of the previous level by a factor of two, after applying a  $5 \times 5$  median filter and a  $5 \times 5$  normal Gaussian filter. The multicascade approach indicates a multistage process, where at each stage the size of the templates is decreased by a factor of two in each dimension. The process starts from the pyramid level with the coarsest resolution images and the cascade stage with the largest size templates. The initial motion vector for each template is calculated. Afterwards, the process is repeated for all combinations of finer resolution images in the pyramid and smaller templates in the cascade, continuously refining the calculated motion vectors. The final step involves the finest resolution image and a number of almost non-overlapping templates of the smallest size. Even in the final cascade stage, the template has >100 pixels, which is enough to provide statistically robust PC and NCC values.

The generated sea ice mask is employed to restrict motion estimation to templates with  $\geq 90\%$  of their area covered by sea ice. In addition, a maximum velocity threshold of 70 cm/s per day is applied, i.e., a drift of 60.48 km/day. Each motion vector with magnitude exceeding this threshold is truncated to 60.48 km/day. As a further post-processing step, a  $6 \times 6$  vector consistency filter is applied, identifying *missing* vectors whose magnitude or direction differs by more than four times the standard deviation of the mean or two times the standard deviation of the median of their neighboring vectors. A  $3 \times 3$  vector median filter is applied in the remaining vectors, whereas fifth-degree 2-D Horner's polynomials are employed to interpolate the missing vectors.

## 4. RESULTS AND DISCUSSIONS

Sea ice motion is estimated for all six consecutive pairs of images, independently for the original-resolution images and their NN upscaled versions. The parameters for pyramid levels and cascade stages applied for each version are: (4, 4) for the original images and (4, 5), (5, 5), and (5, 6) for the upscaled images by two, four, and eight, respectively; in the pair ( $i, j$ ) above,  $i$  represents the number of pyramid levels and  $j$  is the number of cascade stages. The dimensions of the original images are  $608 \times 896$  pixels, and the minimum template size for all image versions is set to  $10 \times 14$  pixels.

The calculated motion vectors from the different image versions are compared against buoys from the International Arctic Buoy Programme (IABP) [14]. The 12:00 GMT reported daily buoy positions and drifts are selected for each date of the imagery and are reprojected to the polar stereo-

<sup>1</sup>[http://suzaku.eorc.jaxa.jp/GCOM.W/data/data\\_w\\_dpss.html](http://suzaku.eorc.jaxa.jp/GCOM.W/data/data_w_dpss.html)

**Table 1.** Accuracy evaluation of the estimated motion vectors from the original (“MCC”) and the upscaled AMSR2 images by a factor of two (“MCC-X2”), four (“MCC-X4”), and eight (“MCC-X8”), against IABP buoys. In total 122 buoy samples are used over the six date pairs. RSE: relative squared error; RMSE: root mean-squared error (in km); MAE: mean absolute error (in km); P: Pearson correlation coefficient.

Versions	RSE	RMSE	MAE	P
x-axis				
MCC	1.110	5.234	3.571	0.490
MCC-X2	1.214	5.475	3.794	0.486
MCC-X4	<b>0.619</b>	<b>3.909</b>	<b>2.786</b>	<b>0.704</b>
MCC-X8	0.850	4.580	2.918	0.571
y-axis				
MCC	0.735	7.054	4.724	0.702
MCC-X2	0.359	4.927	3.644	0.831
MCC-X4	<b>0.266</b>	<b>4.241</b>	<b>3.180</b>	<b>0.890</b>
MCC-X8	0.439	5.450	3.994	0.788

graphic grid of the input data. Each buoy is compared against the nearest estimated vector. For comparison purposes, the same vectors used for the original resolution images are selected for the upscaled versions as well, even though closer vectors to the buoys may exist for the upscaled versions due to their denser vector field. Table 1 reports motion estimation results for several accuracy evaluation measures, in particular the relative squared error (RSE), root mean-squared error (RMSE) in km, mean-absolute error (MAE) in km, and Pearson correlation coefficient (P). As shown in the table, the motion vectors calculated from the upscaled images by a factor of four (“MCC-X4”) are more accurate than all other versions, and significantly better than the original ones. In fact, overall, all upscaled versions perform better than the original resolution by providing vectors with lower errors and higher correlation with the buoy drifts than the original images. Even the upscaled images by a factor of two, that are slightly outperformed by the original ones in the x-axis, provide significantly better results in the y-axis. In addition, it is noteworthy that using the upscaled images by a factor of four significantly outperforms in both axes a previous study [6] employing similar passive microwave 36.5 GHz data and applying oversampling by four in the estimated vectors (RMSE 3.91 km on the x-axis and 4.24 km on the y-axis, contrary to 4.50 km and 4.83 km, respectively, estimated in [6]).

Furthermore, statistics on the error distribution of the motion vectors calculated from the original and upscaled versions are provided in Table 2. In particular, the mean and the standard deviation values over the six date pairs are given, for each image scale. Consistent with the aforementioned results, the upscaled images by four provide the smallest standard de-

**Table 2.** Mean ( $\mu$ ) and standard deviation ( $\sigma$ ) of the errors of the motion vectors calculated from the original and the upscaled AMSR2 images for the six date pairs, for the x- and y-axis.

Versions	$\mu_x$	$\mu_y$	$\sigma_x$	$\sigma_y$
MCC	-0.284	-1.535	5.248	6.913
MCC-X2	<b>-0.079</b>	-0.818	5.497	4.879
MCC-X4	-0.259	<b>-0.485</b>	<b>3.917</b>	<b>4.231</b>
MCC-X8	0.805	1.014	4.527	5.377

viation, i.e., the smallest spread around the mean, among all image versions. They also provide the lowest absolute mean value in the y-axis. On the contrary, the original images result in vectors with the highest standard deviations among all versions, with the only exception being the x-axis results compared with the upscaled images by two.

Figure 1 displays a typical example of the calculated motion vectors for the different data versions. As expected, the upscaled images by four provide motion vectors closely related to the buoy drifts and rather consistent for the overall Arctic region. Relatively consistent results are provided from the rest of the image versions. However, some obvious outliers can still be observed for the upscaled images by two and eight as well as for the original images, e.g., in the Northern Scandinavia (mid-right part of the figure) and North-Eastern Greenland. Although not directly visible from the figure, it is noteworthy that the minimum calculated drift for each image version is one pixel. This demonstrates in practice that even with a simple NN interpolation upscaling, the upscaled images can reduce the quantization error and estimate drifts eight times smaller than the original images, i.e., 1.5625 km contrary to 12.5 km of the original images.

## 5. CONCLUSION

In this paper, we have proposed an approach to estimate sea ice motion at fine scales from passive microwave satellite images. Contrary to previous approaches focusing on embedding upscaling within the already calculated motion vector field to decrease the minimum detected motion, we directly upscale the original satellite images. A hierarchical MCC-based method for motion estimation is applied. Experiments demonstrate that the proposed coupling of a simple NN interpolation upscaling with the MCC method provides motion vectors with higher accuracies than the ones provided by the original images, together with higher resolution of up to eight times and density of up to 64 times ( $8 \times 8$ , for both axes). Upscaling by four outperforms previous study results with embedded oversampling by the same factor. The results open the floor for the investigation of more elaborated image upscaling techniques, such as super-resolution.

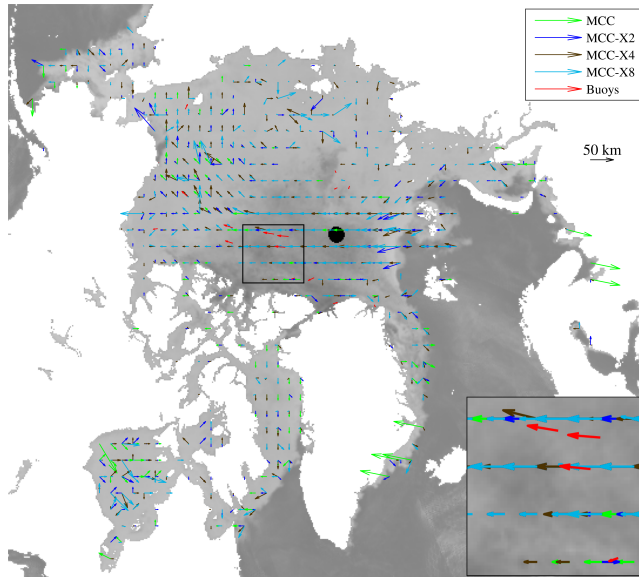


**Fig. 1.** Example of motion vectors estimated from the original and upscaled AMSR2 images for the image pair of January 6–7, 2013. For visualization purposes, a close-up look of the original images is shown, whereas the motion vector distances are magnified by five times. For the same reason, only the estimated vectors on every 8<sup>th</sup> position of the motion vector field calculated by the original images are shown, i.e., 1/8 of the vectors of the original images, and 1/16, 1/32, and 1/64 of the upscaled by two, four, and eight times, respectively, for each axis. Bottom-right corner: a zoom-in view of the black rectangle area.

## 6. ACKNOWLEDGMENT

AMSR2 data was supplied by the GCOM-W1 Data Providing service, Japan Aerospace Exploration Agency (JAXA).

## 7. REFERENCES

- [1] T. Kræmer, H. Johnsen, and C. Brekke, “Emulating Sentinel-1 Doppler radial ice drift measurements using Envisat ASAR data,” *IEEE Trans. Geosci. Remote Sens.*, vol. 53, no. 12, pp. 6407–6418, Dec. 2015.
- [2] G. Spreen, R. Kwok, and D. Menemenlis, “Trends in arctic sea ice drift and role of wind forcing: 1992–2009,” *Geophys. Res. Lett.*, vol. 38, Art. no. L19501, 2011.
- [3] M. Tschudi, C. Fowler, J. Maslanik, J. S. Stewart, and W. Meier, “Polar Pathfinder daily 25 km EASE-Grid sea ice motion vectors, version 3, Daily grids,” Boulder, Colorado USA: National Snow and Ice Data Center, 2016. doi: <http://dx.doi.org/10.5067/O57VAIT2AYYY>. Accessed: Dec. 20, 2016.
- [4] T. Lavergne, S. Eastwood, Z. Teffah, H. Schyberg, and L. A. Breivik, “Sea ice motion from low-resolution satellite sensors: An alternative method and its validation in the Arctic,” *J. Geophys. Res.*, vol. 115, Oct. 2010.
- [5] F. Girard-Ardhuin and R. Ezraty, “Enhanced arctic sea ice drift estimation merging radiometer and scatterometer data,” *IEEE Trans. Geosci. Remote Sens.*, vol. 50, no. 7, pp. 2639–2648, July 2012.
- [6] W. N. Meier and M. Dai, “High-resolution sea-ice motions from AMSR-E imagery,” *Ann. Glaciol.*, vol. 44, pp. 352–356, Nov. 2006.
- [7] M. Thomas, C. Kambhamettu, and C. A. Geiger, “Motion tracking of discontinuous sea ice,” *IEEE Trans. Geosci. Remote Sens.*, vol. 49, no. 12, pp. 5064–5079, Dec. 2011.
- [8] T. Hollands and W. Dierking, “Performance of a multi-scale correlation algorithm for the estimation of sea-ice drift from SAR images: Initial results,” *Ann. Glaciol.*, vol. 52, no. 57, pp. 311–317, May 2011.
- [9] A. S. Komarov and D. G. Barber, “Sea ice motion tracking from sequential dual-polarization RADARSAT-2 images,” *IEEE Trans. Geosci. Remote Sens.*, vol. 52, no. 1, Jan. 2014.
- [10] R. Kwok, D. A. Schweiger, D. A. Rothrock, S. Pang, and C. Kottmeier, “Sea ice motion from satellite passive microwave imagery assessed with ERS SAR and buoy motions,” *J. Geophys. Res.*, vol. 103, no. C4, pp. 8191–8214, Apr. 1998.
- [11] National Snow and Ice Data Center, “Documentation: Polar stereographic projection and grid,” [Online]. Available: <http://nsidc.org/data/polar-stereo/ps-grids.html>. Accessed: May 12, 2017.
- [12] National Ice Center (NIC) and NSIDC. 2010, updated daily, “Multisensor Analyzed Sea Ice Extent Northern Hemisphere. Sea Ice Extent 4 km,” Developed by F. Fetterer, M. Savoie, S. Helfrich, and P. Clemente-Coln. Boulder, Colorado USA: National Snow and Ice Data Center. <http://dx.doi.org/10.7265/N5GT5K3K>. Accessed: Dec. 20, 2016.
- [13] Z. I. Petrou and Y. Tian, “High-resolution sea ice motion estimation with optical flow using satellite spectroradiometer data,” *IEEE Trans. Geosci. Remote Sens.*, vol. 55, no. 3, pp. 1339–1350, Mar. 2017.
- [14] M. Tschudi, C. Fowler, J. Maslanik, J. S. Stewart, and W. Meier, “Polar Pathfinder daily 25 km EASE-Grid sea ice motion vectors, version 3, Buoys,” Boulder, Colorado USA: National Snow and Ice Data Center, 2016. doi: <http://dx.doi.org/10.5067/O57VAIT2AYYY>. Accessed: Dec. 20, 2016.